HHS Public Access

Author manuscript

J Am Chem Soc. Author manuscript; available in PMC 2021 February 05.

Published in final edited form as:

J Am Chem Soc. 2020 February 05; 142(5): 2601–2608. doi:10.1021/jacs.9b12693.

Capture and Release of Singlet Oxygen in Coordination-Driven Self-Assembled Organoplatinum(II) Metallacycles

Yan-Qin He[†,‡,⊥], **Werner Fudickar**[§,⊥], **Jian-Hong Tang**[*,‡], **Heng Wang**[‖], **Xiaopeng Li**[‖], **Jun Han**[†], **Zhengping Wang**[†], **Min Liu**[†], **Yu-Wu Zhong**[#], **Torsten Linker**[*,§], **Peter J. Stang**[*,‡]

[†]Institute of BioPharmaceutical Research, Liaocheng University, 1 Hunan Road, Liaocheng, Shandong 252059, China

[‡]Department of Chemistry, University of Utah, 315 South 1400 East, Room 2020, Salt Lake City, Utah 84112, United States

[§]Department of Chemistry, University of Potsdam, Karl-Liebknecht-Str. 24–25, 14476 Potsdam, Germany

[‖]Department of Chemistry, University of South Florida, 4202 East Fowler Avenue, Tampa, Florida 33620, United States

[#]Key Laboratory of Photochemistry, Beijing National Laboratory for Molecular Sciences, CAS Research/Education Center for Excellence in Molecular Sciences, Institute of Chemistry, Chinese Academy of Sciences, Beijing 100190, China

Abstract

Singlet oxygen ($^1O_2$), as an important active reagent, has found wide applications in photodynamic therapy (PDT), synthetic chemistry and materials science. Organic conjugated aromatics serving as hosts to capture and release singlet oxygen have been systematically investigated over the last decades. Herein, we present a [6+6] organoplatinum(II) metallacycle by using ~180° dipyridylanthracene donor and ~120° Pt(II) acceptor as the building blocks, which enables the capture and release of singlet oxygen with relatively high photooxygenation and thermolysis rate constants. The photooxygenation of the metallacycle to the corresponding endoperoxide was performed by sensitized irradiation, and the resulting endoperoxide is stable at room temperature and can be stored under ambient condition over months. Upon simple heating the neat endoperoxide under inert atmosphere at 120 °C for 4 h, the resulting endoperoxide can be reconverted to the corresponding parent form and singlet oxygen. The photooxygenation and thermolysis products were characterized by NMR spectroscopy and ESI-TOF-MS analysis. Density functional theory calculations were conducted in order to reveal the frontier molecular orbital interactions and reactivity. This work provides a new material-platform for singlet oxygen related promising applications.

[*]**Corresponding Author:** u6014248@utah.edu, linker@uni-potsdam.de, stang@chem.utah.edu.

[⊥]These authors contributed equally to this work.

Supporting Information

The Supporting Information is available free of charge on the ACS Publications website at DOI:

Additional experimental data and characterization spectra, including Table S1 - S2 and Figures S1 – S12.

The authors declare no competing financial interest.

Graphical Abstract

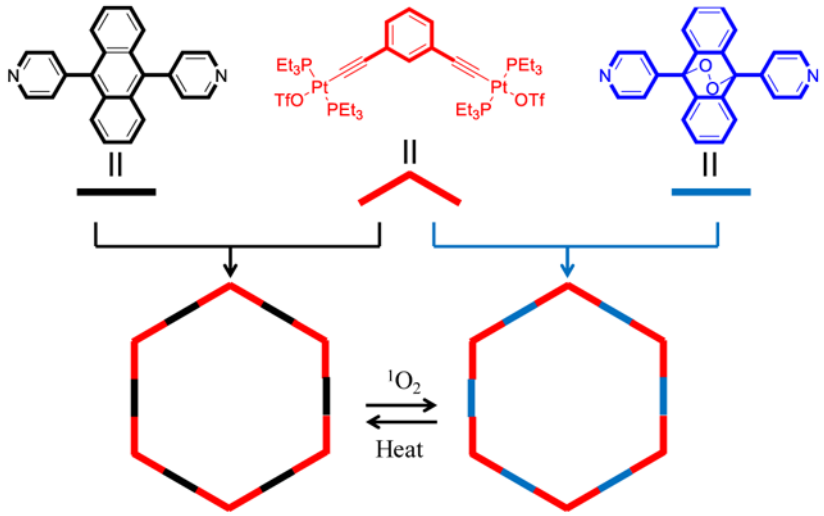

INTRODUCTION

Singlet oxygen ($^1O_2$) is a metastable excited state of molecular oxygen with the ability to oxidize organic and biological compounds, providing a wide range of applications in synthetic organic chemistry,[1,2] materials science[3–12] and photodynamic therapy (PDT).[13–18] In general, there are two methods to generate singlet oxygen via the energy transfer based photoexcitation of ground-state oxygen (photosensitization), or as a product in a chemical reaction.[19–22] In the photosensitization of ground-state oxygen approach, a photosensitizer is photoexcited by light and then sensitizing the neigh-bouring ground-state oxygen to produce singlet oxygen. However, the photooxygenation technique involves some practical and technical challenges, especially for using on a large scale, such as the requirement of the simultaneous presence of molecular oxygen and a photosensitizer, light penetration of the reaction media, and the limited solubility of the molecular oxygen in solution. Another chemical method is also known as “dark” oxygenation, which is a promising alternative to address the controllable generation of singlet oxygen. Traditionally, the H_2O_2/catalyst and HOCl/catalyst based inorganic systems rely on cheap reagents and yield singlet oxygen quantitively, but typically require an aqueous media condition and show cytotoxicity to the cells. Recently, specific aromatic organic compounds have been reported to react with singlet oxygen to form the corresponding endoperoxides (EPOs), such as naphthalene, 2-pyridones and anthracene derivatives.[2,23–29] Many kinds of EPOs are able to convert back to the parent aromatic organic compounds and singlet oxygen under external thermal, photo or chemical stimuli, which allow a clean generation of singlet oxygen without remaining oxidation reagents and sensitizers, and are not restricted to the aqueous media. The reversibility of the reaction allows applications of EPOs in the area of singlet oxygen storage, fluorescent photo-switching and photodynamic therapy. We found that the reactivity of the anthracene-based EPOs is dependent on the substituents and the chemical conditions.[30,31] For instance, kinetics of the ortho, meta, and para isomers of 9,10-dipyridylanthracene are controlled by the substitution pattern and solvent.[32] By using a simple chemical trigger

at low temperature, the release of the reactive singlet oxygen from dipyridylanthracene EPOs in aqueous media has also been found.[25] Besides that, some EPOs are not stable at room temperature. The development of room temperature stable EPOs is still highly desired for the application of singlet oxygen storage.[33,34] Moreover, the reported EPOs are mainly based on the polycyclic aromatic hydrocarbons systems, which are still unexplored in the field of the discrete organic-inorganic hybrid frameworks.

Supramolecular coordination complexes (SCCs) arising from the methodology of coordination-driven self-assembly via the formation of metal-ligand bonds between the electron-poor metal acceptors and the rigid electron-rich organic donors, display attractive features such as well-defined shapes and sizes, facile building block functionalization and modularity, and increased solubilities.[35–45] A large number of functional SCCs have been produced for applications in host–guest chemistry, materials sciences and medical sciences, including two-dimensional (2D) metallacycles and three dimensional (3D) metallacages.[38,46–53] Very recently, an elegant dual-stage metallacycle by using a $^1O_2$ generation porphyrin photosensitizer and diarylethene photochromic switch as the functional building blocks was reported, which shows the capability to reversibly control $^1O_2$ generation via photosensitization.[54]

Herein, we present a new discrete [6+6] organoplatinum(II) metallacycle containing six ~180° dipyridylanthracene responsive moieties, which are introduced to allow the capture and release of singlet oxygen in the multi reaction sites. Upon the photooxygenation process, the six anthracene groups in a discrete metallacycle skeleton react with singlet oxygen to afford the metallacycle endoperoxide (M-EPO). The obtained M-EPO is stable under ambient condition and can be stored over months. By using the dipyridylanthracene endoperoxide ligand as the starting material, the corresponding M-EPO can also be prepared by coordination-driven self-assembly. The release of singlet oxygen from the M-EPO was performed by heating the M-EPO solid at 120 °C for 4 h under inert condition, which was determined by adding a $^1O_2$ trap reagent. Accordingly, the reversible capture and release of singlet oxygen in an organoplatinum(II) metallacycle are achieved, which provides a promising alternative for the polycyclic aromatic hydrocarbons singlet oxygen reactive reagents.

RESULTS AND DISCUSSION

Synthesis and Characterization.

The organic ligands **1**and **3** were prepared according to our previous published procedures.[32] Based on the coordination-driven self-assembly methodology, the pyridyl groups terminated 180 ° organic donor ligands (**1**, **3**) react with 120° diplatinum(II) acceptor (**2**) to afford [6+6] metallacycles **4** and **5**. For **4**, the reaction was conducted in CH_2Cl_2/CH_3OH (1/1, v/v) at 50 °C for 10 h. Under similar conditions, metallacycle **5** was synthesized by stirring the starting materials at room temperature. The metallacycles were characterized by multinuclear NMR (^{1}H NMR, $^{31}P\{^1H\}$ NMR, ^{13}C NMR) and electrospray ionization time-of-flight mass spectrometry (ESI-TOF-MS) analysis. As shown in the ^{1}H NMR spectra of metallacycles **4** and **5** (Figure 2a), the peaks corresponding to the H_α and H_β protons of the pyridine groups show downfield shifts as compared to the spectra of the free ligands **1** and **3** ($\Delta\delta = -0.47$,

−0.52 ppm for the H_α, H_β of **4**, Δδ = −0.46, −0.47 ppm for the H_α, H_β of **5**, respectively), indicating the formation of Pt-pyridyl coordination bonds. In the $^{31}P\{^1H\}$ NMR spectra of **4** and **5** (Figure 2b), the sharp singlets (ca. 16.72 ppm for **4**, 17.54 ppm for **5**) with concomitant ^{195}Pt satellites (J_{Pt-P} = 2294.9 Hz for **4** and 2294.5 Hz for **5**) are observed for each of the metallacycles corresponding to a single phosphorus environment. Compared to the precursor Pt(II) acceptor **2**, these peaks show an upfield shift by approximately 5.52 and 4.70 ppm for **4** and **5**, respectively. Metallacycles **4** and **5** were also studied by ^{13}C NMR. As shown in (Figure S7), the ^{13}C NMR spectrum of **5** exhibits a characteristic peak at 83.26 ppm, suggesting the existence of C-O bonds. This signal is not observed in the ^{13}C NMR spectrum of **4**.

ESI-TOF-MS is a well established technique to provide evidence for the stoichiometric formation of the multi-charged supramolecular coordination complexes. As shown in Figures 2c, 2d, a series of mass peaks (from 6+ to 9+) owing to the loss of different numbers of trifluoromethanesulfonate groups (OTf^-) are found in the ESI-TOF-MS spectra of **4** and **5**. The isotopically resolved peaks with seven positive charges ($[M - 7OTf]^{7+}$) at m/z = 1237.21 for **4**, 1264.63 for **5** are in agreement with their calculated theoretical distributions (Figure S3, S6), further supporting the formation of the discrete [6+6] metallacyclic assemblies.

Spectroscopic characterizations.

As shown in Figure 3a, UV–Vis absorption of metallacycle **4** displays the intense vibronic band at 340–450 nm arising from the anthracene moieties. In contrast, this band is absent in the absorption spectrum of M-EPO **5** due to the formation of endoperoxide, which is consistent with the changes of the precursor ligand **1** and **3**.[32] The emission spectra of **4** and **5** show a similar phenomenon (Figure 3b). Metallacycle **4** is moderately emissive in acetone with the emission quantum yield of ca. 0.23. However, no obvious emission band was observed in the solution of M-EPO **5** under the same conditions. The distinct differences of the spectroscopic behaviors between **4** and M-EPO **5** afford a facile technique for monitoring the reaction of singlet oxygen and provide potential application in the responsive switches.

Photooxygenation of 4.

Compound **4** was rapidly photooxygenated to the corresponding endoperoxide (**5'**) in CD_3OD (40 mg/4 mL), using methylene blue as sensitizer. The obtained product was studied by NMR spectroscopic (^1H NMR, $^{31}P\{^1H\}$ NMR, ^{13}C NMR), ESI-TOF-MS and UV-vis spectral analysis. As shown in Figures 4, S7, the ^1H NMR, $^{31}P\{^1H\}$ NMR and ^{13}C NMR spectra of endoperoxide (**5'**) are in agreement with that of the as-prepared complex **5**. The formation of **5'** was further determined by ESI-TOF-MS analysis. ESI-TOF-MS signals of **5'** at m/z = 1087.81, 1264.63 and 1500.40 were observed (Figure S8), which are consistent with the mass spectral results of the as-prepared complex **5**. Hence, the photooxygenation of compound **4** affords the endoperoxide (**5'**) with the same molecular structure as complex **5**.

UV/vis measurements were conducted to monitor the photooxygenation of **4** in methanol (or MeOH) under solution under *pseudo* first order reactions conditions (see experimental

details in the SI). As shown in Figure S9, the absorption band at 340–450 nm gradually decreased during irradiation. To classify the reactivity of complex **4**, we performed an analogous irradiation experiment with just the precursor ligand **1**, which has been investigated in our previous work.[32] It's worth noting that complex **4** consists of six reacting anthracene moieties, while the ligand **1** has one anthracene group. Thus, to compare the reactivity of **1** and **4**, concentrations were employed at a ratio of 6:1 for **1** and **4** respectively. Complex **4** shows a slower absorption decay at the characteristic band (340–450 nm) than the precursor ligand **1** (Figure 5). The slope fits reveal a ratio of ~2/1 between the reactivity of **1** and **4**. The reduced reactivity of the complex can be ascribed to the appearance of the positive charges, which reduce the electron density of the reaction center. This behavior is in accordance with our previous studies on acceptor substituents at diarylanthracenes.[55] To further prove such influences, we also conducted the irradiation experiment with the positively charged methylated form **1-Me^{2+}** (Figure 5). In this case the conversion proceeded significantly slower ($k_{\mathbf{1\text{-}Me2^{+}}}/k_{\mathbf{4}}$~1/3.6). Thus, metal coordination of the pyridyl site reduces electron density to a minor extend as compared to covalent binding to a methyl group. Since the slope of the complex remains linear until completion, we can conclude that each anthracene moiety within the complex reacts independently with the absence of allosteric effects.

To investigate the reaction possibility of Pt-phosphine ligand with singlet oxygen,[56,57] the control experiments by using a precursor ligand **6** without anthracene units were performed. In this precursor ligand **6**, the labile OTf terminal groups of 120° diplatinum(II) acceptor (**2**) were replaced by iodide units. Under the similar photooxygenation conditions, there is no obvious shifts in ^{31}P NMR Spectra of **6** before and after irradiation (Figure S10), indicating a lack of reactivity between Pt-phosphine ligand and singlet oxygen.

Theoretical calculations.

The reactivity of [4+2] cycloadditions between anthracenes and $^{1}O_2$ can be predicted by the frontier molecular orbital (FMO) theory, based on the energy arising from the overlap between the *termini* of a diene and a dienophile.[58] The FMO theory indeed indicated a good correlation between the energy of the HOMO of an acene as diene and the rate constant of its reaction with $^{1}O_2$.[30,55,59–62]

Therefore, with the intention to explain the reduced rate of the complex **4** relative to ligand **1** and its enhanced reactivity relative to the cationic ligand **1-Me^{2+}**, DFT calculations of **1**, **1-Me^{2+}** and the model structure **6** holding the anthracene ligand **1** and two [$(PMe_3)_2$Pt(C≡CPh)] units, were performed on a B3LYP(LANL2DZ/6–31G*) level. Populations of the resulting frontier orbitals with their energies are shown in Figure 6. Interestingly, their HOMOs are differently populated: While the HOMOs of the bare ligand **1** and the cationic species **1-Me^{2+}** show maximal density on the anthracene units, as is typical for anthracenes,[30] the maximal population of the HOMO of complex **6** is situated at the outer two ethynylphenyl units. TDDFT calculations further reveal that the first excited state of the complex **6** correspond to a charge transfer from these peripheral units into the LUMO (Table S1) at a wavelength of 442 nm, which is consistent with the red-shift in the UV/vis spectrum of **4** as compared to the free ligand **1** (Figure S11). The reason for the swap

of the two orbital populations is that the pyridyl groups of **6** transfer partial charge from the anthracene moiety *via* the metal center towards the alkynyl moiety (see Mulliken charge populations in Figure S12). As a consequence of this difference, the [4+2] $^1O_2$ cycloaddition of **6** *cannot* occur from its HOMO.

The highest occupied orbital of model complex **6**, which shows maximum population at the acene core lies energetically below the HOMO (HOMO–1) with an energy of −9.41 eV. HOMO–1 of **6** lies energetically between the HOMO energies of **1** and **1-Me^{2+}**, which is in line with the order of reactivities (Figure 6). In summary, FMO theory revealed that the calculated energies of the pertinent orbitals of the diene and the reactivities correlate well. Thus, *N*-metal coordination causes weaker stabilization of the acene towards $^1O_2$ than the direct introduction of a formal positive charge at the nitrogen atom.

Thermolysis of the endoperoxides. The solid of the obtained endoperoxide 5’ and as-prepared complex 5 was directly heated at 120 °C for 4 h with no solvent to fully regenerate the parent complex (4’). Complex 4’ was characterized by ^{1}H NMR, ^{31}P{^{1}H} NMR, and ESI-TOF-MS analysis. As shown in Figure 6, upon heating complex 5 at 120 °C in an inert atmosphere for 4 h, the ^{1}H NMR and ^{31}P{^{1}H} NMR of 4’ exhibit the characteristics of complex 4. ESI-TOF-MS spectrum of 4’ shows a series of mass peaks at m/z = 928.95, 1040.32 and 1468.43 (Figure S13). These mass signals can also be observed in the mass spectrum of compound 4 (Figure S3), which further confirm the reconversion of the M-EPO.

An investigation of the reconversion M-EPO kinetics was complicated by the lack of a suitable solvent, in which the complex remained stable. High boiling solvents such as DMF or DMSO, cause the decomposition of the complex. However, we could investigate the reconversion of M-EPO by multiple cycles of heating the neat sample followed by measuring the UV/vis absorption spectrum in a defined volume of acetone and removal of solvent. As shown in Figure 8, the kinetics follows a clean first order process with a half-life of 2.6 h at 90°C. Thus, the M-EPO **5** reconverts significantly faster to its parent form than the free ligand EPO **3** (9.6 h at 90°C).[32] Its worth noting that the complex remained stable throughout the thermolysis process since no traces of free ligand **1** were found in the ^{1}H NMR or UV/vis-spectra.

Release of Singlet Oxygen.

In order to verify that a fraction of the released oxygen is in its singlet state, a solution of the $^1O_2$ trapping reagent 1,3-diphenylisobenzofurane (DPBF) in toluene was added to the M-EPO. By measuring the DPBF absorbance at 413 nm, a full consumption of the trap was observed upon heating a tenfold excess of the M-EPO **5** at 110 °C (Figure 9). To quantify the amount of $^1O_2$ released per M-EPO complex, transfer experiments to DPBF were performed with an excess of the trapping reagent in deuterated solvent in order to keep the fraction of $^1O_2$ solvent quenching as low as possible. The average of these experiments revealed that 28±4% of the released oxygen is in its excited state.

CONCLUSION

In summary, we have prepared two supramolecular metallacycles by the coordination-driven self-assembly of a ~120° Pt(II) acceptor with a ~180° dipyridyl donor or its corresponding endoperoxide. As the comparative study with the corresponding as-prepared endoperoxide shows, the reversible capture and release of singlet oxygen was realized in this multidipyridylanthracene-bridged organoplatinum(II) metallacycle. The products of the photooxygenation and thermolysis were fully characterized by a combination of NMR experiments and ESI-TOF-MS measurements. UV/vis analysis provides further kinetic results about the photooxygenation and thermolysis of the metallacycle, indicating that the photooxygenation kinetic rate constant of the metallacycle lies between the rate constant of the free ligand and the rate of its corresponding dicationic form **1-Me**$^{2+}$. The thermolysis of the resulting M-EPO affords re-generation of the parent complex under release of singlet oxygen. Moreover, a faster re-generation of singlet oxygen from the M-EPO **5** is observed compared to the free ligand EPO **3**. This work paves a new pathway to achieve the reversible capture and release of singlet oxygen by using supramolecular coordination complexes.

EXPERIMENTAL SECTION

Materials and Methods.

All reagents were commercially available and used as supplied without further purification (I assume that they are still available). ^{1}H NMR and ^{13}C NMR spectra were recorded on a Varian Inova 500 MHz spectrometer. ^{31}P{^{1}H} NMR spectra were measured on a Varian Unity 300 MHz spectrometer, using an external unlocked sample of 85% H_3PO_4 (δ = 0) as reference. ESI-TOF-MS were recorded on a Waters Synapt G2 mass spectrometer. Absorption and fluorescence spectra were recorded on a Hitachi U-4100 and Hitachi F-7000 Spectrophotometer, equipped with 1 cm quartz cuvettes from Starna Cells, Inc. DFT and TDDFT calculations were carried out using the B3LYP exchange correlation function and implemented in the *Gaussian* 09 package.[62]

Synthesis of 4.

9,10-Bis(4-pyridyl)anthracene (**1**, 3.32 mg, 10.0 μmol) and **2** (12.85 mg, 10.0 μmol) were mixed in CH_2Cl_2/CH_3OH (3 mL/3 mL). The resulting solution was stirred at 50 °C for 10 h. After cooling to rt, the system was then concentrated by flushing with N_2 gas. The resulting yellow solid was collected without further purification to give compound **1** in quantitative yield (>99%). ^{1}H NMR (500 MHz, Acetone-d_6): δ 9.37 (d, *J* = 7.5 Hz, 24H), 8.04 (d, *J* = 7.0 Hz, 24H), 7.56–7.65 (m, overlapped, 48H), 7.44 (s, 6H), 7.33–7.34 (m, overlapped, 18H), 2.15–2.18 (m, overlapped, 144H), 1.32–1.40 (m, overlapped, 216H). ^{31}P{^{1}H} NMR (121.4 MHz, Acetone-d_6): *δ* 16.72 (s, ^{195}Pt satellites, $^{1}J_{Pt–P}$ = 2294.9 Hz). ESI-TOF-MS calcd for $[M – 7OTf]^{7+}$ (m/z): 1237.21. Found: 1237.21.

Synthesis of 5.

Complex **5** was prepared under the similar procedure for the synthesis of **4**. Ligands **2** and **3** were stirred in CH_2Cl_2/CH_3OH (3 mL/3 mL) at room temperature for 10 h to afford the white solid product **5** in quantitative yield (>99%). ^{1}H NMR (500 MHz, Acetone-d_6): δ 9.38

(d, J = 8.0 Hz, 24H), 8.15 (d, J = 8.5 Hz, 24H), 7.22–7.41 (m, overlapped, 72H), 2.08–2.12 (m, overlapped, 144H), 1.27–1.38 (m, overlapped, 216H). $^{31}P\{^{1}H\}$ NMR (121.4 MHz, Acetone-d_6): δ 17.01 (s, ^{195}Pt satellites, $^{1}J_{Pt-P}$ = 2294.5 Hz). ESI-TOF-MS calcd for [M – 7OTf]$^{7+}$ (m/z): 1264.78. Found: 1264.77.

Preparative photooxygenation of 4 to give 5'.

To a solution of complex **4** in CD_3OD (40 mg/4 mL) in a pyrex glass tube was added methylene blue (1 mg). The tube was irradiated for 30 min by using a 300 W sodium lamp at 5 °C, while oxygen was bubbled through the solution.

Supplementary Material

Refer to Web version on PubMed Central for supplementary material.

ACKNOWLEDGMENT

P.J.S. thanks the NIH (R01-CA215157) for financial support. X.L. is thankful for financial support from NIH (R01GM128037). We also thank the Doctoral Foundation of Liaocheng University (318051646), Open Project of Shandong Collaborative Innovation Center for Antibody Drugs (CIC-AD1838) and Taishan scholar research Foundation. This work was also supported by Shandong Collaborative Innovation Center for Antibody Drugs and Engineering Research Center for Nanomedicine and Drug Delivery Systems. T. L. and W. F. thank the University of Potsdam for financial support.

REFERENCES

(1). Ghogare AA; Greer A Using Singlet Oxygen to Synthesize Natural Products and Drugs. Chem. Rev 2016, 116, 9994–10034. [PubMed: 27128098]

(2). Aubry JM; Pierlot C; Rigaudy J; Schmidt R Reversible Binding of Oxygen to Aromatic Compounds. Acc. Chem. Res 2003, 36, 668–675. [PubMed: 12974650]

(3). Ogilby PR Singlet Oxygen: There is Indeed Something New under the Sun. Chem. Soc. Rev 2010, 39, 3181–3209. [PubMed: 20571680]

(4). Gao Z; Han YF; Wang F Cooperative Supramolecular Polymers with Anthracene-Endoperoxide Photo-Switching for Fluorescent anti-Counterfeiting. Nat. Commun 2018, 9 3977. [PubMed: 30266899]

(5). Fan XY; Wang YY; Deng L; Li L; Zhang XF; We P Oxidative Capacity Storage of Transient Singlet Oxygen from Photosensitization with a Redox Mediator for Improved Chemiluminescent Sensing. Anal. Chem 2019, 91, 9407–9412. [PubMed: 31272151]

(6). Liu KL; Lalancette RA; Jakle F B-N Lewis Pair Functionalization of Anthracene: Structural Dynamics, Optoelectronic Properties, and O-2 Sensitization. J. Am. Chem. Soc 2017, 139, 18170–18173. [PubMed: 29185739]

(7). Zhou Y; Zhang HY; Zhang ZY; Liu Y Tunable Luminescent Lanthanide Supramolecular Assembly Based on Photoreaction of Anthracene. J. Am. Chem. Soc 2017, 139, 7168–7171. [PubMed: 28509539]

(8). Adam W; Kazakov DV; Kazakov VP Singlet-Oxygen Chemiluminescence in Peroxide Reactions. Chem. Rev 2005, 105, 3371–3387. [PubMed: 16159156]

(9). Filatov MA; Karuthedath S; Polestshuk PM; Savoie H; Flanagan KJ; Sy C; Sitte E; Telitchko M; Laquai F; Boyle RW; Senge MO Generation of Triplet Excited States via Photoinduced Electron Transfer in meso-anthra-BODIPY: Fluorogenic Response toward Singlet Oxygen in Solution and in Vitro. J. Am. Chem. Soc 2017, 139, 6282–6285. [PubMed: 28407710]

(10). Mahne N; Schafzahl B; Leypold C; Leypold M; Grumm S; Leitgeb A; Strohmeier GA; Wilkening M; Fontaine O; Kramer D; Slugovc C; Borisov SM; Freunberger SA Singlet Oxygen Generation as a Major Cause for Parasitic Reactions During Cycling of Aprotic Lithium-Oxygen Batteries. Nat. Energy 2017, 2 17036.

(11). Wang H; Yang XZ; Shao W; Chen SC; Xie JF; Zhang XD; Wang J; Xie Y Ultrathin Black Phosphorus Nanosheets for Efficient Singlet Oxygen Generation. J. Am. Chem. Soc 2015, 137, 11376–11382. [PubMed: 26284535]

(12). Park J; Feng DW; Yuan S; Zhou HC Photochromic Metal-Organic Frameworks: Reversible Control of Singlet Oxygen Generation. Angew. Chem. Int. Ed 2015, 54, 430–435.

(13). Di Mascio P; Martinez GR; Miyamoto S; Ronsein GE; Medeiros MHG; Cadet J Singlet Molecular Oxygen Reactions with Nucleic Acids, Lipids, and Proteins. Chem. Rev 2019, 119, 2043–2086. [PubMed: 30721030]

(14). Mroz P; Yaroslavsky A; Kharkwal GB; Hamblin MR Cell Death Pathways in Photodynamic Therapy of Cancer. Cancers. 2011, 3, 2516–2539. [PubMed: 23914299]

(15). Jiao L; Zhang XY; Cui JN; Peng XJ; Song FL Three-in-One Functional Silica Nanocarrier with Singlet Oxygen Generation, Storage/Release, and Self-Monitoring for Enhanced Fractional Photodynamic Therapy. ACS Appl. Mater. Interfaces 2019, 11, 25750–25757. [PubMed: 31245990]

(16). Benz S; Notzli S; Siegel JS; Eberli D; Jessen HJ Controlled Oxygen Release from Pyridone Endoperoxides Promotes Cell Survival under Anoxic Conditions. J. Med. Chem 2013, 56, 10171–10182. [PubMed: 24299550]

(17). Kolemen S; Ozdemir T; Lee D; Kim GM; Karatas T; Yoon J; Akkaya EU Remote-Controlled Release of Singlet Oxygen by the Plasmonic Heating of Endoperoxide-Modified Gold Nanorods: Towards a Paradigm Change in Photodynamic Therapy. Angew. Chem. Int. Ed 2016, 55, 3606–3610.

(18). Yuan YY; Zhang CJ; Xu SD; Liu B A Self-Reporting AIE Probe with a Built-in Singlet Oxygen Sensor for Targeted Photodynamic Ablation of Cancer Cells. Chem. Sci 2016, 7, 1862–1866. [PubMed: 29899908]

(19). Fudickar W; Linker T Release of Singlet Oxygen from Organic Peroxides under Mild Conditions. Chemphotochem. 2018, 2, 548–558.

(20). Martins S; Farinha JPS; Baleizao C; Berberan-Santos MN Controlled Release of Singlet Oxygen Using Diphenylanthracene Functionalized Polymer Nanoparticles. Chem. Commun 2014, 50, 3317–3320.

(21). Elsherbini M; Allemann RK; Wirth T “Dark” Singlet Oxygen Made Easy. Chem. Eur. J 2019, 25, 12486–12490. [PubMed: 31373412]

(22). Ghorai P; Dussault PH A New Peroxide Fragmentation: Efficient Chemical Generation of O-1(2) in Organic Media. Org. Lett 2009, 11, 4572–4575. [PubMed: 19772310]

(23). Turro NJ; Chow MF; Rigaudy J Mechanism of Thermolysis of Endoperoxides of Aromatic Compounds. Activation Parameters, Magnetic Field, and Magnetic Isotope Effects. J. Am. Chem. Soc 1981, 103, 7218–7224.

(24). Noh T; Gan H; Halfon S; Hrnjez BJ; Yang NCC Chemistry of *Anti*-o,o’-dibenzene. J. Am. Chem. Soc 1997, 119, 7470–7482.

(25). Fudickar W; Linker T Release of Singlet Oxygen from Aromatic Endoperoxides by Chemical Triggers. Angew. Chem. Int. Ed 2018, 57, 12971–12975.

(26). Liu KL; Lalancette RA; Jakle F Tuning the Structure and Electronic Properties of B-N Fused Dipyridylanthracene and Implications on the Self-Sensitized Reactivity with Singlet Oxygen. J. Am. Chem. Soc 2019, 141, 7453–7462. [PubMed: 30998336]

(27). Turan IS; Yildiz D; Turksoy A; Gunaydin G; Akkaya EU A Bifunctional Photosensitizer for Enhanced Fractional Photodynamic Therapy: Singlet Oxygen Generation in the Presence and Absence of Light. Angew. Chem. Int. Ed 2016, 55, 2875–2878.

(28). Wasserman HH; Scheffer JR Singlet Oxygen Reactions from Photoperoxides. J. Am. Chem. Soc 1967, 89, 3073–3075.

(29). Xiao WY; Wang P; Ou CJ; Huang XY; Tang YY; Wu MY; Si WL; Shao JJ; Huang W; Dong XC 2-Pyridone-Functionalized Aza-BODIPY Photosensitizer for Imaging-Guided Sustainable Phototherapy. Biomaterials. 2018, 183, 1–9. [PubMed: 30142531]

(30). Fudickar W; Linker T Why Triple Bonds Protect Acenes from Oxidation and Decomposition. J. Am. Chem. Soc 2012, 134, 15071–15082. [PubMed: 22881365]

(31). Klaper M; Fudickar W; Linker T Role of Distance in Singlet Oxygen Applications: A Model System. J. Am. Chem. Soc 2016, 138, 7024–7029. [PubMed: 27187766]

(32). Fudickar W; Linker T Synthesis of Pyridylanthracenes and Their Reversible Reaction with Singlet Oxygen to Endoperoxides. J. Org. Chem 2017, 82, 9258–9262. [PubMed: 28759234]

(33). Erbas-Cakmak S; Akkaya EU Toward Singlet Oxygen Delivery at a Measured Rate: A Self-Reporting Photosensitizer. Org. Lett 2014, 16, 2946–2949. [PubMed: 24849844]

(34). Martinez GR; Ravanat JL; Medeiros MHG; Cadet J; Di Mascio P Synthesis of a Naphthalene Endoperoxide as a Source of O^{18} Labeled Singlet Oxygen for Mechanistic Studies. J. Am. Chem. Soc 2000, 122, 10212–10213.

(35). Cook TR; Zheng YR; Stang PJ Metal-Organic Frameworks and Self-Assembled Supramolecular Coordination Complexes: Comparing and Contrasting the Design, Synthesis, and Functionality of Metal-Organic Materials. Chem. Rev 2013, 113, 734–777. [PubMed: 23121121]

(36). Oliveri CG; Ulmann PA; Wiester MJ; Mirkin CA Heteroligated Supramolecular Coordination Complexes Formed via the Halide-Induced Ligand Rearrangement Reaction. Acc. Chem. Res 2008, 41, 1618–1629. [PubMed: 18642933]

(37). Oh M; Carpenter GB; Sweigart DA Supramolecular Metal-Organometallic Coordination Networks Based on Quinonoid π-Complexes. Acc. Chem. Res 2004, 37, 1–11. [PubMed: 14730989]

(38). Chen LJ; Yang HB Construction of Stimuli-Responsive Functional Materials via Hierarchical Self-Assembly Involving Coordination Interactions. Acc. Chem. Res 2018, 51, 2699–2710. [PubMed: 30285407]

(39). Rizzuto FJ; von Krbek LKS; Nitschke JR Strategies for Binding Multiple Guests in Metal-Organic Cages. Nat. Rev. Chem 2019, 3, 204–222.

(40). De S; Mahata K; Schmittel M Metal-Coordination-Driven Dynamic Heteroleptic Architectures. Chem. Soc. Rev 2010, 39, 1555–1575. [PubMed: 20419210]

(41). Gan MM; Liu JQ; Zhan L; Wang YY; Hahn FE; Han YF Preparation and Post-Assembly Modification of Metallosupramolecular Assemblies from Poly(N-Heterocyclic Carbene) Ligands. Chem. Rev 2018, 118, 9587–9641. [PubMed: 29975040]

(42). Fujita M; Tominaga M; Hori A; Therrien B Coordination Assemblies from a Pd (II)-Cornered Square Complex. Acc. Chem. Res 2005, 38, 369–378. [PubMed: 15835883]

(43). Zhang HC; Lee J; Brewster JT; Chi XD; Lynch VM; Sessler JL Cation-based Structural Tuning of Pyridine Dipyrrolate Cages and Morphological Control over Their Self-assembly. J. Am. Chem. Soc 2019, 141, 4749–4755. [PubMed: 30813734]

(44). Wu GY; Chen LJ; Xu L; Zhao XL; Yang HB Construction of Supramolecular Hexagonal Metallacycles via Coordination-Driven Self-Assembly: Structure, Properties and Application. Coord. Chem. Rev 2018, 369, 39–75.

(45). Chen L; Chen QH; Wu MY; Jiang FL; Hong MC Controllable Coordination-Driven Self-Assembly: From Discrete Metallocages to Infinite Cage-Based Frameworks. Acc. Chem. Res 2015, 48, 201–210. [PubMed: 25517043]

(46). Saha R; Devaraj A; Bhattacharyya S; Das S; Zangrando E; Mukherjee PS Unusual Behavior of Donor-Acceptor Stenhouse Adducts in Confined Space of a Water-Soluble Pd-8(II) Molecular Vessel. J. Am. Chem. Soc 2019, 141, 8638–8645. [PubMed: 31050889]

(47). Cook TR; Stang PJ Recent Developments in the Preparation and Chemistry of Metallacycles and Metallacages via Coordination. Chem. Rev 2015, 115, 7001–7045. [PubMed: 25813093]

(48). Shi BB; Liu YZ; Zhu HTZ; Vanderlinden RT; Shangguan LQ; Ni RD; Acharyya K; Tang JH; Zhou ZX; Li XP; Huang FH; Stang PJ Spontaneous Formation of a Cross-Linked Supramolecular Polymer Both in the Solid State and in Solution, Driven by Platinum(II) Metallacycle-Based Host-Guest Interactions. J. Am. Chem. Soc 2019, 141, 6494–6498. [PubMed: 30966741]

(49). Zhang ZY; Zhao ZQ; Hou YL; Wang H; Li XP; He G; Zhang MM Aqueous Platinum(II)-Cage-Based Light-Harvesting System for Photocatalytic Cross-Coupling Hydrogen Evolution Reaction. Angew. Chem. Int. Ed 2019, 58, 8862–8866.

(50). Yan XZ; Cook TR; Wang P; Huang FH; Stang PJ Highly Emissive Platinum(II) Metallacages. Nat. Chem 2015, 7, 342–348. [PubMed: 25803473]

(51). Li B; He T; Fan YQ; Yuan XC; Qiu HY; Yin SC Recent Developments in the Construction of Metallacycle/metallacage-cored Supramolecular Polymers via Hierarchical Self-assembly. Chem. Commun 2019, 55, 8036–8059.

(52). Gao WX; Zhang HN; Jin GX Supramolecular Catalysis Based on Discrete Heterometallic Coordination-driven Metallacycles and Metallacages. Coord. Chem. Rev 2019, 386, 69–84.

(53). Chakraborty S; Newkome GR Terpyridine-Based Metallosupramolecular Constructs: Tailored Monomers to Precise 2D-motifs and 3D-metallocages. Chem. Soc. Rev 2018, 47, 3991–4016. [PubMed: 29594272]

(54). Qin Y; Chen LJ; Dong FY; Jiang ST; Yin GQ; Li XP; Tian Y; Yang HB Light-Controlled Generation of Singlet Oxygen within a Discrete Dual-Stage Metallacycle for Cancer Therapy. J. Am. Chem. Soc 2019, 141, 8943–8950. [PubMed: 31088049]

(55). Fudickar W; Linker T Remote Substituent Effects on the Photooxygenation of 9,10-Diarylanthracenes: Strong Evidence for Polar Intermediates. Chem. Commun 2008, 1771–1773.

(56). Ho DG; Gao R; Celaje J; Chung H-Y; Selke M, Phosphadioxirane: A peroxide from an ortho-substituted arylphosphine and singlet dioxygen. Science 2003, 302, 259–262. [PubMed: 14551430]

(57). Greer A, A view of unusual peroxides. Science 2003, 302, 235–236. [PubMed: 14551422]

(58). Fleming I Molecular Orbitals and Organic Chemical Reactions; John Wiley & Sons: West Sussex, 2009; p 224.

(59). Chien SH; Cheng MF; Lau KC; Li WK Theoretical Study of the Diels-Alder Reactions between Singlet Oxygen and Acenes. J. Phys. Chem. A 2005, 109, 7509–7518. [PubMed: 16834120]

(60). Vandenheuvel CJM; Verhoeven JW; Deboer TJ A Frontier Orbital Description of the Reaction of Singlet Oxygen with Simple Aromatic Systems. Recl. Trav. Chim. Pays-Bas 1980, 99, 280–284.

(61). Klaper M; Linker T New Singlet Oxygen Donors Based on Naphthalenes: Synthesis, Physical Chemical Data, and Improved Stability. Chem. Eur. J 2015, 21, 8569–8577. [PubMed: 25919359]

(62). Hay PJ; Wadt WR Ab Initio Effective Core Potentials for Molecular Calculations. Potentials for K to Au Including the Outermost Core Orbitals. J. Chem. Phys 1985, 82, 299–310.

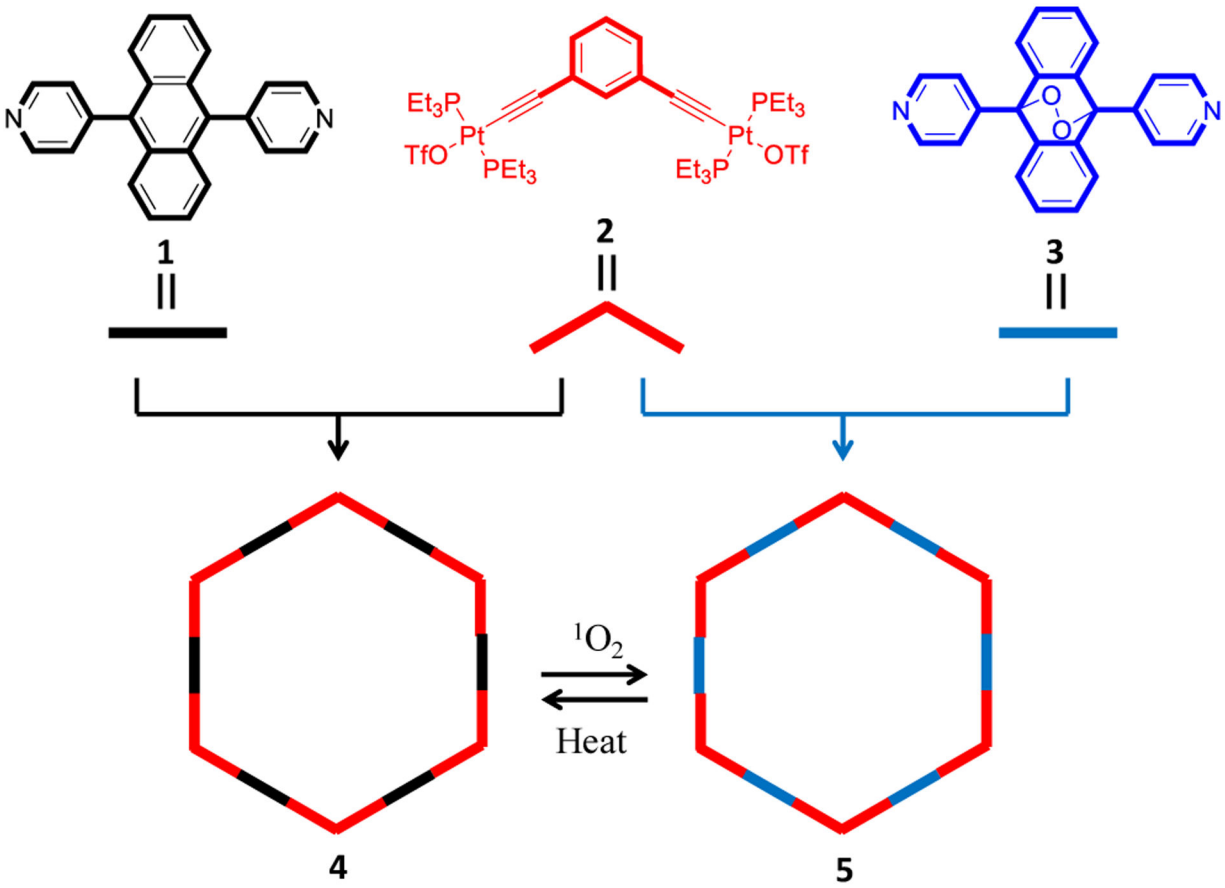

Figure 1.
Synthetic routes to metallacycles **M1** and **M2**.

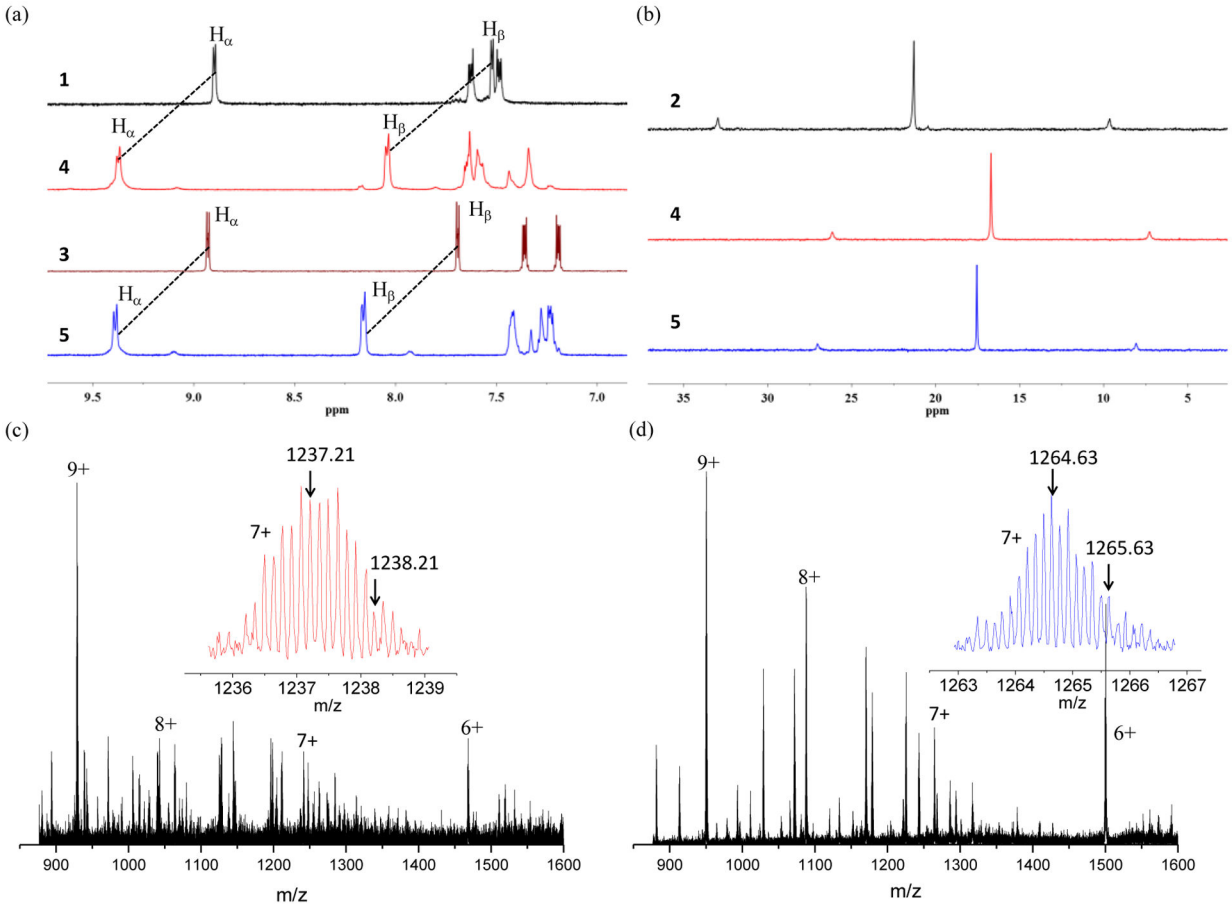

Figure 2.

(a) Partial ^{1}H NMR (500 MHz, acetone-d_6, 298 K), (b) $^{31}P\{^{1}H\}$ NMR (121.4 MHz, acetone-d_6, 298 K) and (c, d) ESITOF-MS spectra of compounds studied in this work.

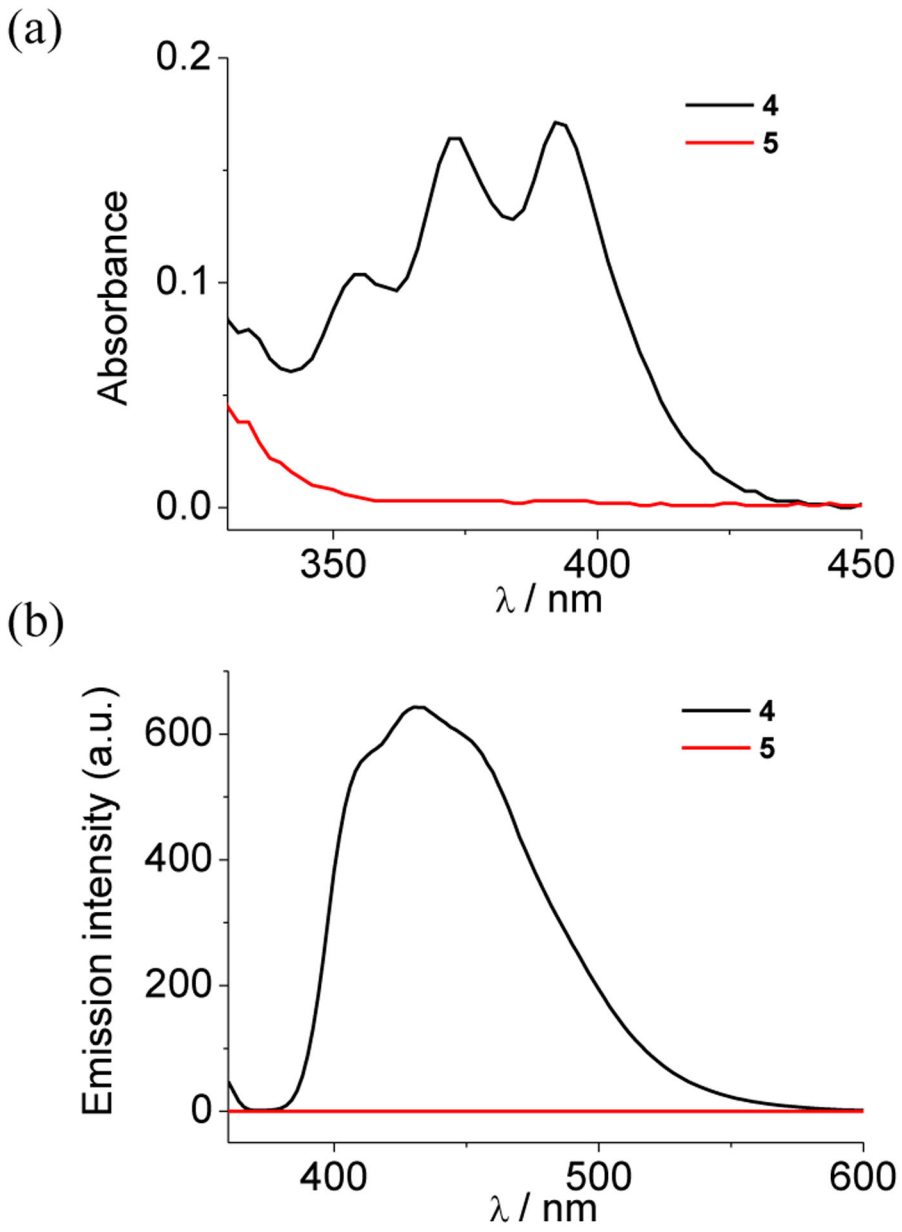

Figure 3.

(a) Absorption and (b) emission spectra of **4** and **5** in acetone ($c = 2.0 \times 10^{-6}$ M, $\lambda_{ex} = 350$ nm).

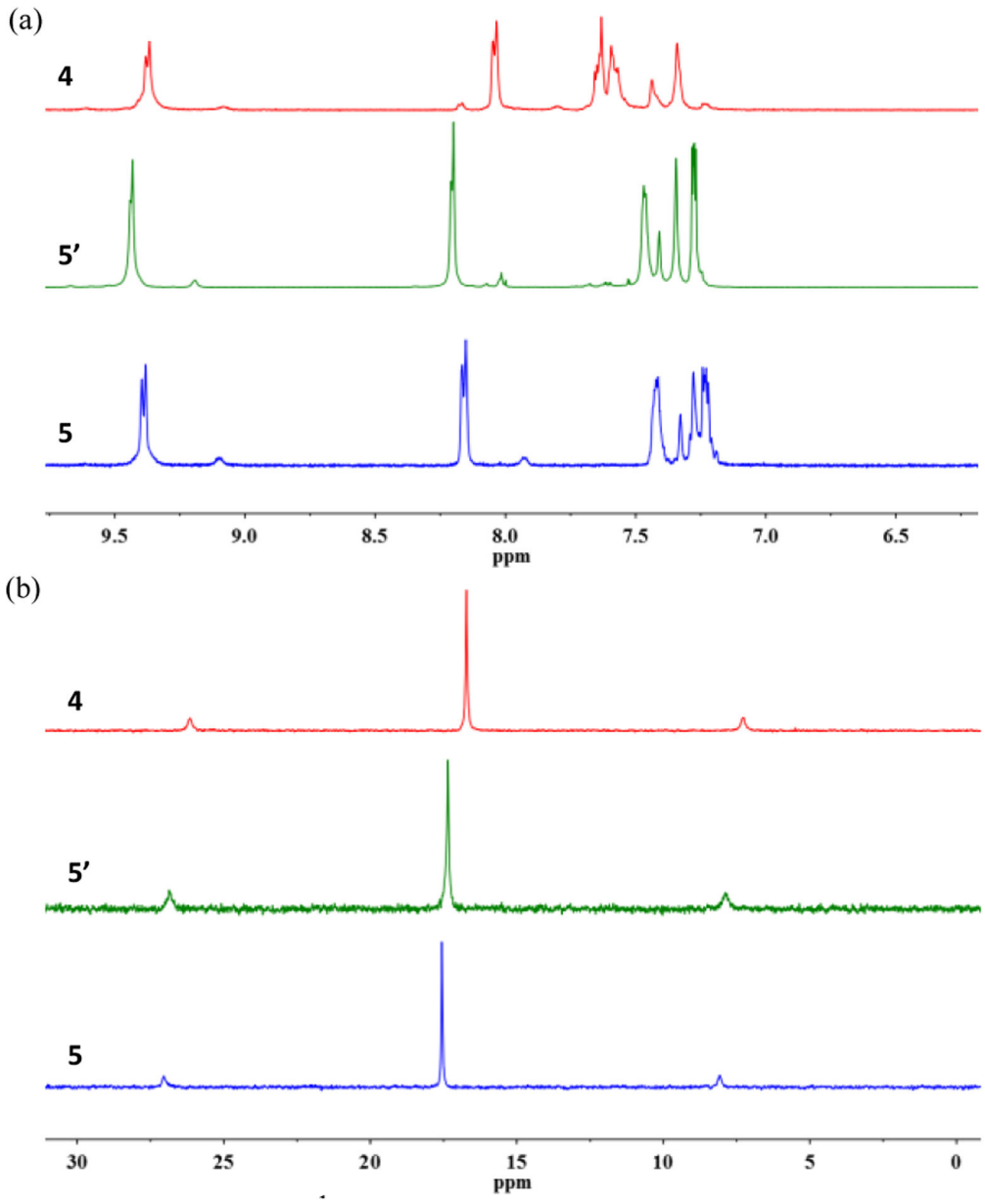

Figure 4.

Partial (a) ^{1}H NMR (500 MHz, acetone-d_6, 298 K) and (b) $^{31}P\{^{1}H\}$ NMR (121.4 MHz, acetone-d_6, 298 K) of complexes **4**, **5'**, **5**.

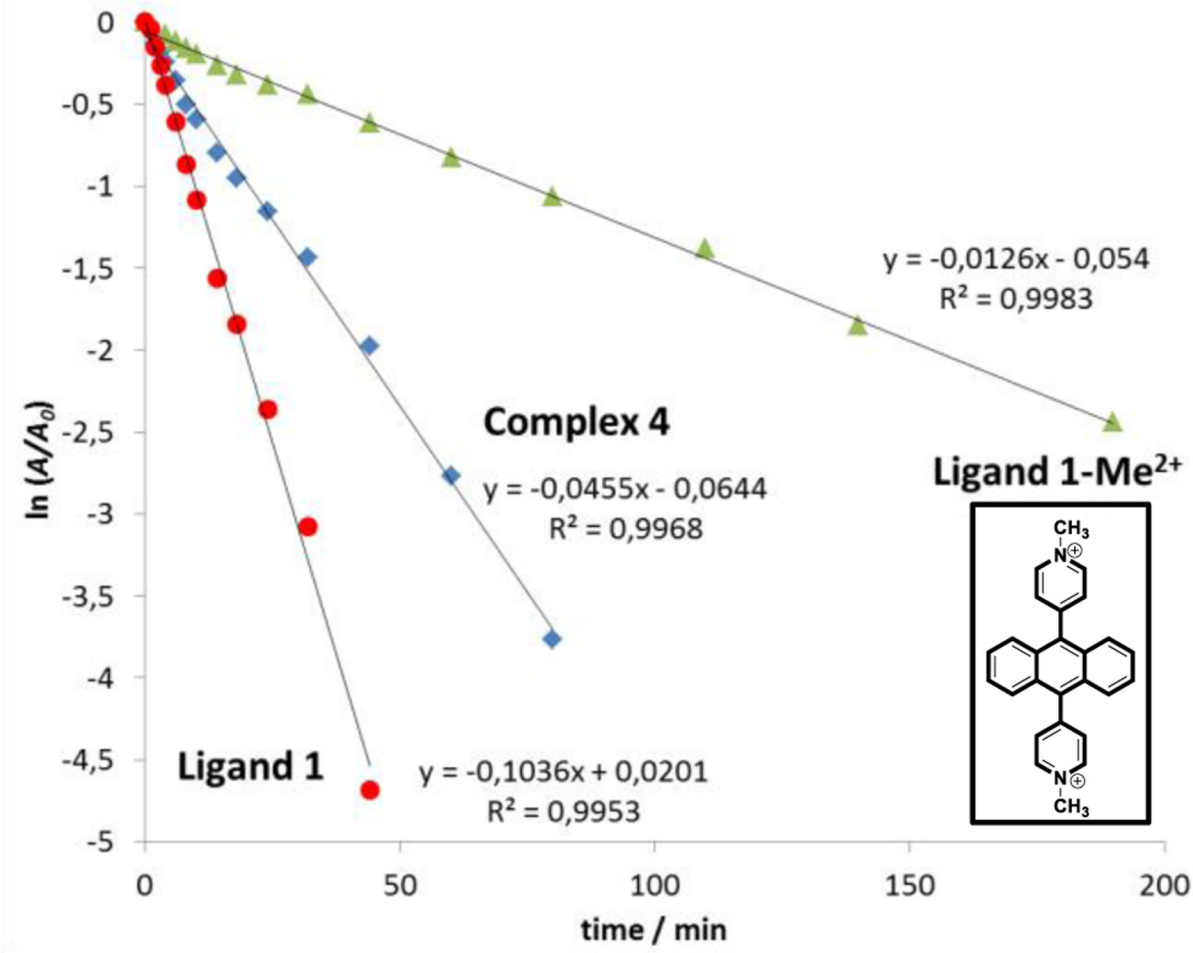

Figure 5.

The absorbance decays of complex **4**, ligand **1** and its cationic methylated form **1-Me^{2+}** caused by photooxygenation in CD_3OD, depicted as semilogarithmic plots.

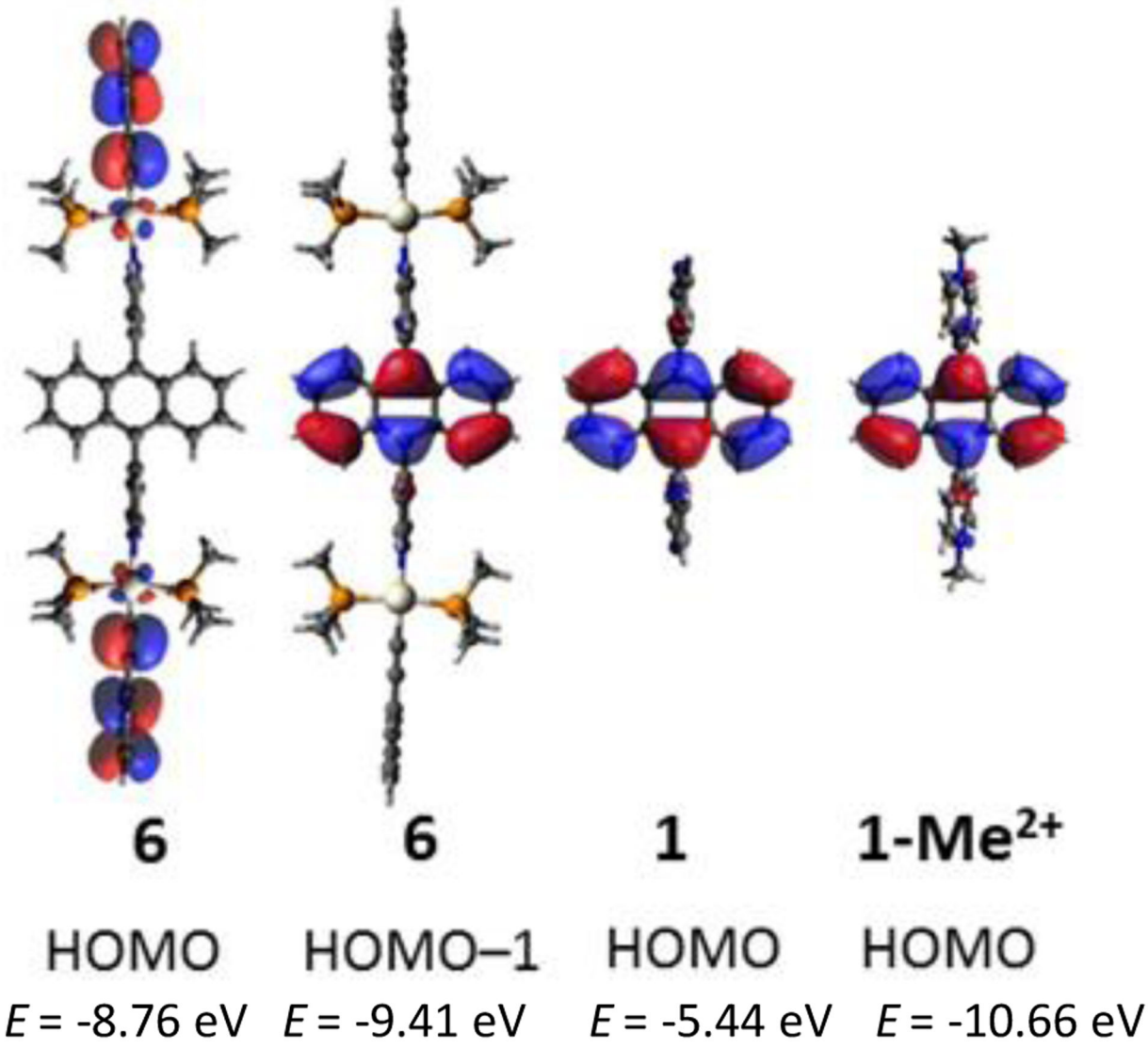

Figure 6.

Populations and energies of the HOMOs and HOMO–1 of the model complex **6**, the ligand **1** and its methylated cationic form **1-Me^{2+}**.

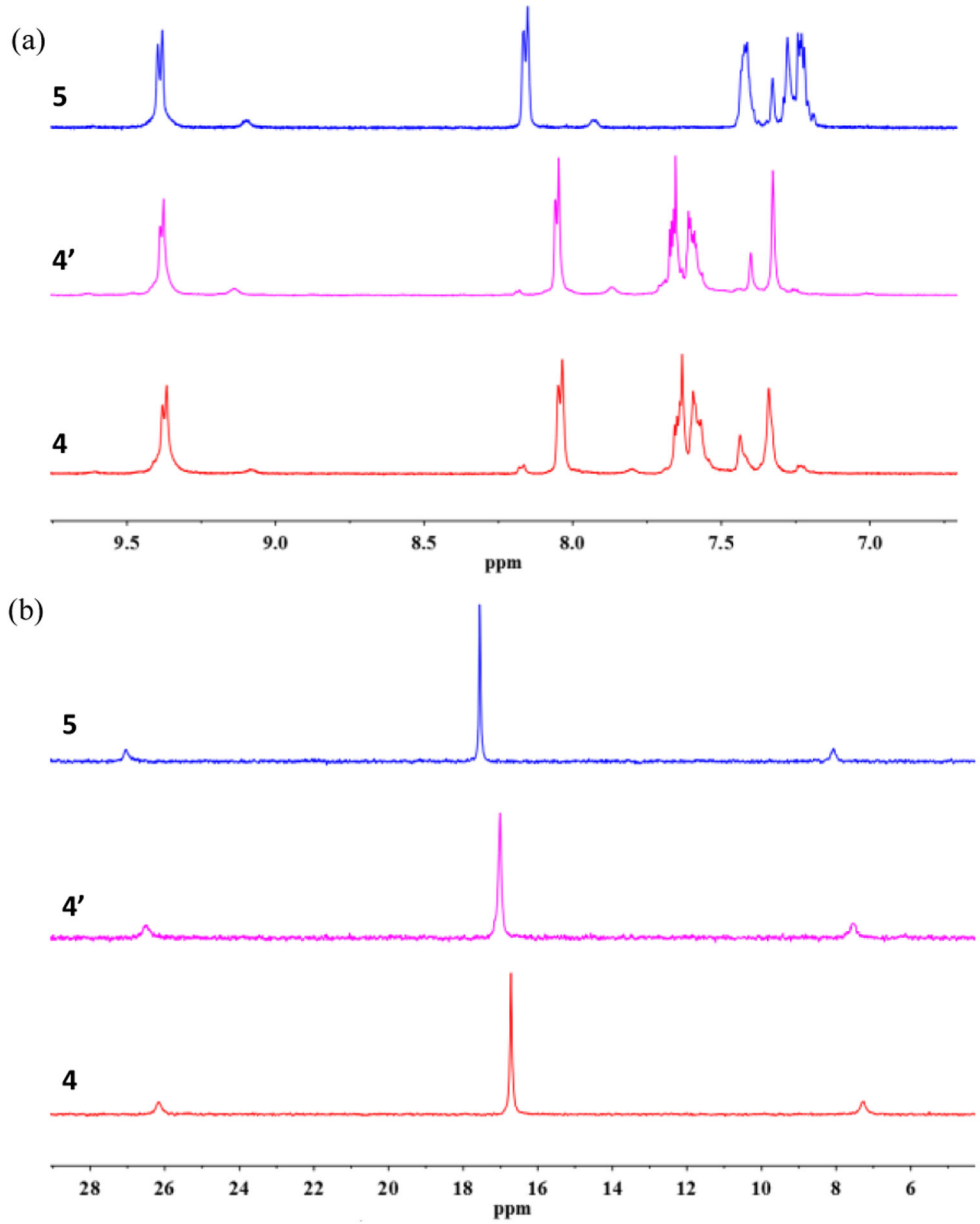

Figure 7.

Partial (a) ^{1}H NMR (500 MHz, acetone-d_6, 298 K) and (b) $^{31}P\{^{1}H\}$ NMR (121.4 MHz, acetone-d_6, 298 K) of complexes **5**, **4'**, **4**.

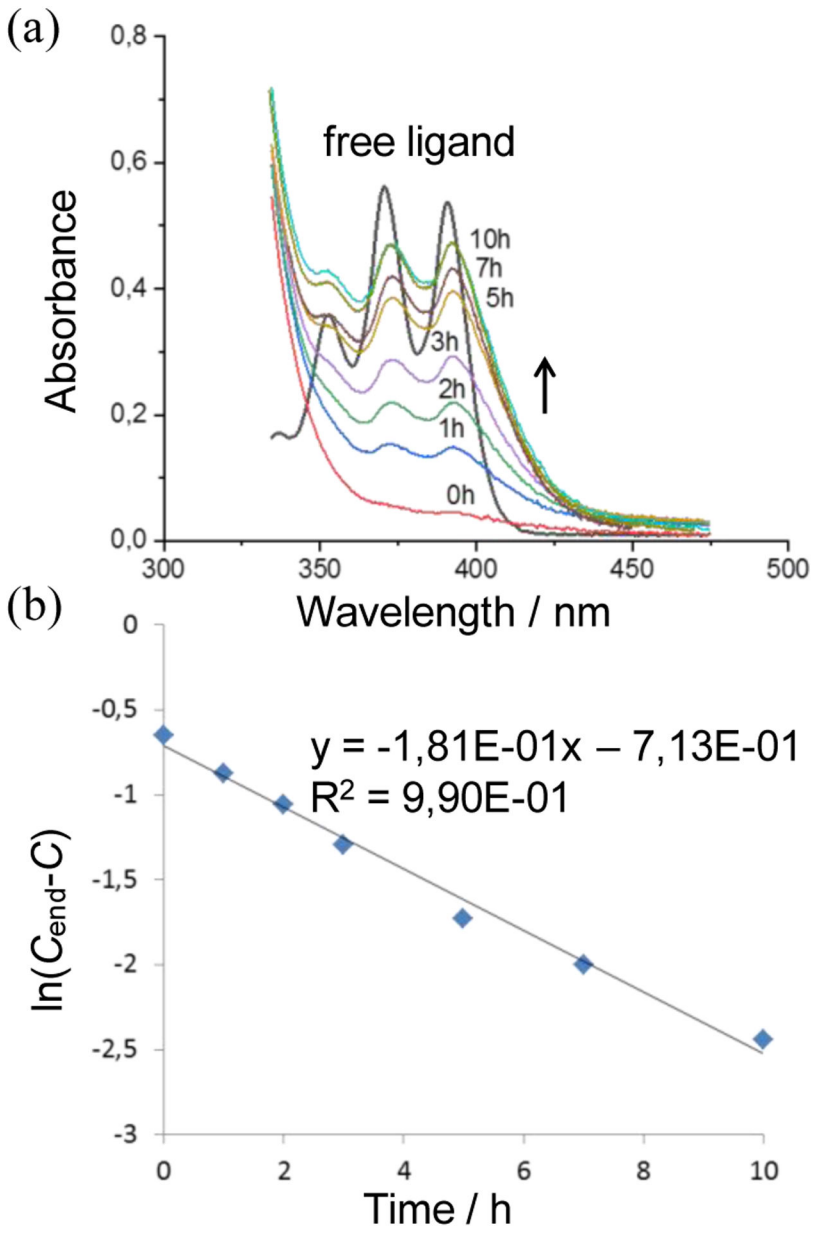

Figure 8.

(a) UV/vis spectra showing the reappearance of **4'** upon heating of **5** (colored curves) and the free ligand **1** for comparison; (b) semi-logarithmic plot of disappearing M-EPO **5** as derived from the absorbances.

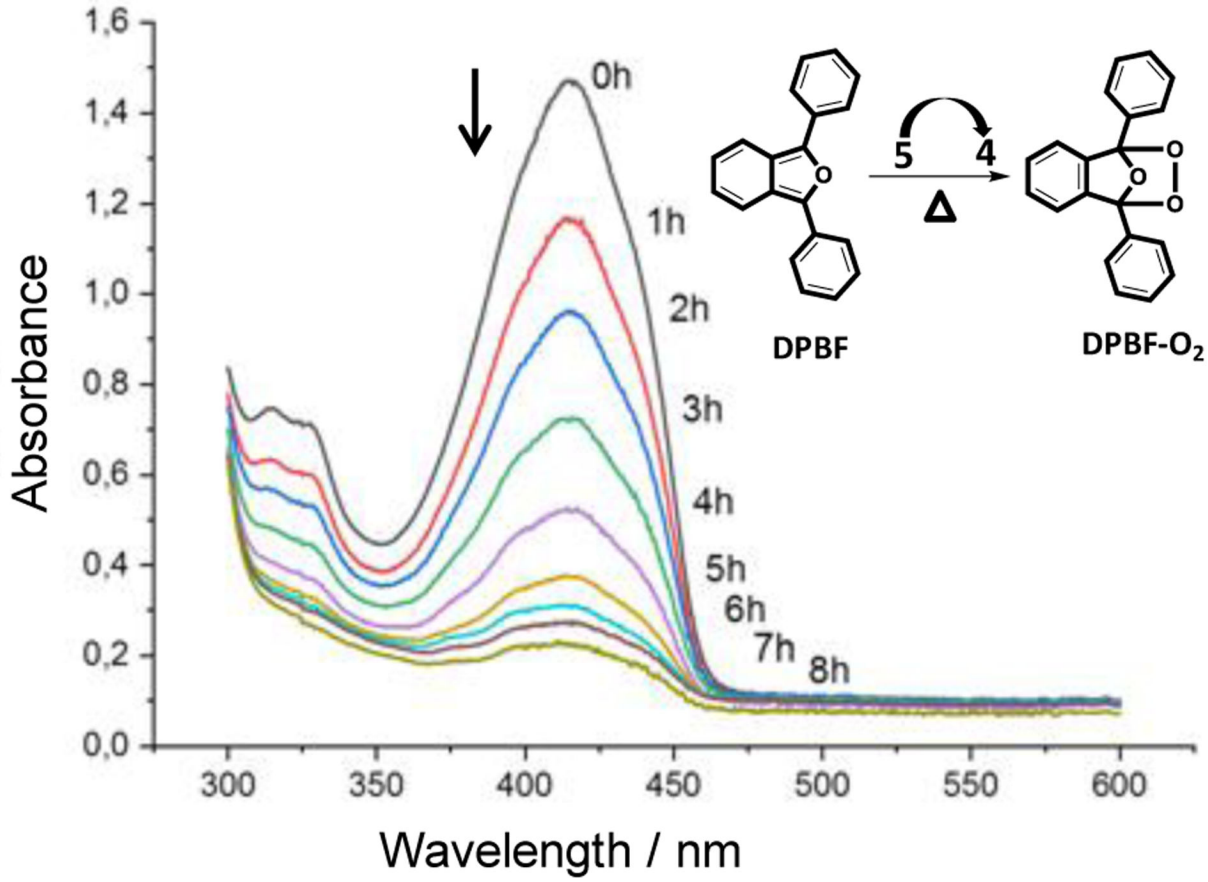

Figure 9.
Reaction of DPBF with $^1O_2$ generated upon thermolysis of the M-EPO **5.**